

# The Integrated Satellite Observation SIMulator for a Coherent Doppler Lidar (ISOSIM-L)

P. Baron<sup>1</sup>, S. Ishii<sup>1</sup>, K. Mizutani<sup>1</sup>, T. Itabe<sup>1</sup>, M. Yasui<sup>1</sup>

<sup>1</sup>National Institute of information and Communications Technology (NICT), Koganei, Japan  
email: baron@nict.go.jp

**Abstract:** The Integrated Satellite Observation SIMulator for Coherent Doppler Lidar (ISOSIM-L) is a comprehensive model developed in the National Institute of Information and Communications Technology (NICT) to study the performances of a coherent Doppler lidar for observing atmospheric winds from an aircraft or space. We describe the latest version of the model which has been implemented by Fujitsu-FIP under a NICT contract. After a brief introduction to explain our motivations, the principles of the wind measurements are given. The main characteristics of the model as well as an example are described. We conclude by providing several points to be improved in the future.

## 1. Introduction

Most of the tropospheric winds measurements used in meteorological and global circulation models are performed in meteorological stations (surface measurements or balloon sondes) which are restricted to land area, mainly in the northern hemisphere. Additional measurements are also available from ground-based radar, data from commercial civil aircraft (e.g., AMDAR program) or satellite observations of the motion of atmospheric structures (e.g., clouds). Global winds measurements have been called to cover missing area such as ocean, tropics and high-latitudes regions. Spaceborne lidar is particularly well suited to provide global wind profiles with high vertical resolution [1, 8]. The European Space Agency (ESA) has chosen the Atmospheric Dynamics Mission-AEOLUS as an Earth Explorer core mission and plans to launch the satellite in late 2013 [6]. The mission uses a direct detection lidar at  $0.355 \mu\text{m}$  and a single line-of-sight perpendicular to the orbit in order to measure the line-of-sight wind up to 20 km.

In Japan, the National Institute of Information and Communications Technology (NICT) has developed a coherent (heterodyne) Doppler wind lidar at  $2 \mu\text{m}$  which has been tested for ground-based observations [4]. Studies are also being conducted to apply such technology to a spaceborne platform (see the presentation from Ishii et al. in this issue). To support the definition of such instrument, the Integrated

Satellite Observation SIMulator for Coherent Doppler Lidar (ISOSIM-L) has been developed. One of our objectives is to collaborate with other institutes to integrate the simulator into an Observing System Simulation Experiments (OSSE) in order to properly characterize what could be the impact of the measurements on the performances of the atmospheric models.

The simulator describes in a comprehensive way, the observations by one or two lidars aboard a moving platform (aircraft, satellite) of a 3-D atmosphere in the infra-red spectral domain (eye safe domain). It predicts for each laser shot and for each time gate, the direct outputs of the receiver as a time function of the digitized photo-current (current waveform) and its spectrum, the mean signal power, the signal-to-noise ratio and the wind retrieval error. The computations includes the satellite motion and attitude jitter, a 3-D representation of the aerosols and clouds distribution, the solar radiance reflected in the line-of-sight for the day and the time of the simulation, and take into account the Earth surface characteristics (elevation and type) at the geographical position observed by the lidars. Note that the simulator can also run in a simplified static and 1-D mode for obtaining quick results (setting and computation). In the next sections of this presentation we will focus on the 3-D mode of ISOSIM-L.

## 2. Observation principles

Figure 1 (left panel) shows a schematic view of

the observation principle using co-aligned emitter and detector beams. Laser pulses are repeatedly emitted with a known wavelength along a line-of-sight slightly off the nadir (e.g.,  $35^\circ$  for AEOLUS). For a coherent detector, the photons received from the atmosphere are mixed with a local-oscillator (LO) and converted to a RF electric current. The photo-current has a mean power proportional to the atmospheric signal power, and beats at a frequency equal to frequency difference between the atmospheric signal and the LO. The RF current is digitized and analyzed by Fourier transform within time gates of few microseconds. For each time gate, the frequency difference with the known incident pulse is derived using statistical method to locate the signal line in the noisy spectrum. After the correction of the satellite motion and the Earth rotation, the Doppler shift is converted to the mean line-of-sight atmospheric wind  $v$  in the range gate:

$$v = \frac{\lambda \delta\nu}{2}$$

where  $\lambda$  is the wavelength of the incoming laser pulse,  $\delta\nu$  is the measured frequency shift of the returned signal and the factor 2 is to account for the double Doppler shift that occurs when the air-mass is scattered and when the return signal is detected.

A vertical profile is derived from a single shot (the maximum length of the profiles is given by half of the time separation of two pulses) and the vertical resolution is defined by the time gate duration  $T$ :  $dR = c\frac{T}{2}$ , where  $c$  is the light velocity. Using a second telescope pointing in a perpendicular direction, the orthogonal component of the horizontal wind can also be measured in the same air slab along the platform trajectory.

The error on the retrieved velocity is dependent on the algorithm used for finding the position of the spectral line in the noisy spectrum. In ISOSIM-L, the error is that given by the pulse pair algorithm [5]:

$$\delta\nu = \frac{\lambda}{4\pi} \left( \frac{f_s}{2NLT} \right)^{1/2} \left( 2\pi^{2/3}W + \frac{16\pi^2W^2}{SNR} + \frac{1}{SNR^2} \right)^{1/2} \cdot \quad (1)$$

where  $SNR$  is the signal to noise ratio,  $f_s$  is the sampling frequency,  $T$  is the time gate duration,  $N$  is the number of averaged pulses,  $L$  is gate-range length to the pulse length ratio,  $W$  is the measure of the frequency spread of the noise-free atmospheric signal given by  $\frac{\sqrt{v_{bw}^2 + v_{atm}^2}}{v_{Ny}}$  with  $v_{Ny} = f\lambda/2$  is the maximum unaliased velocity,  $v_{bw} = \frac{\lambda}{4\pi T}$  is the velocity

uncertainty corresponding to the bandwidth of the transmitted pulse (Gaussian shape) and  $v_{atm}$  is the standard deviation of the velocity distribution in the volume of air.

The receiver noise ( $N$ ) is dominated by the shot-noise:  $N = \frac{\eta_{het}\lambda}{hcB}$  with  $B = T/2$  is the noise equivalent bandwidth and  $\eta_{het}$  is the heterodyne quantum efficiency.

### 3. Model description

The left panel of Fig. 1 shows the different components of the model. User parameters allow to set the period and the GMT time of the simulation as well as the satellite motion and jitters, the pointing direction and the instrumental characteristics. The simulator uses a 3-D representation of the atmospheric states including aerosols and liquid clouds. Optical properties for aerosols and clouds are given as the complex refractive index for each material types. The molecular absorption coefficients are pre-calculated at the model grid points.

Given the atmospheric states along the line-of-sight and the observation characteristics, the model computes the received power and the SNR for each laser shot and for each range gate. Then, the corresponding waveform  $i_s(t)$  and the spectrum of the digitized current are computed. The intensity of the waveform depends on the power  $P$  of the signal backscattered by molecules-aerosols-clouds, and reflected by the surface:

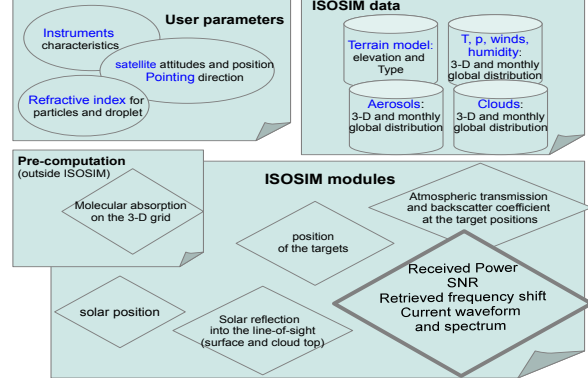
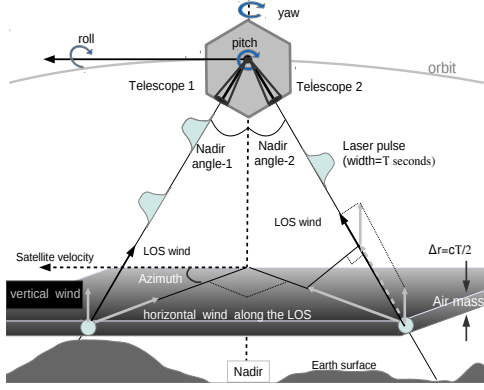
$$i_s(t) \propto \sqrt{P_{cloud} + P_{aer} + P_{mol} + P_{surf}}.$$

The waveform calculation takes into account the frequency shift induced by the atmospheric winds and the platform velocity as well as the thermal random distribution of the velocities within the gate range and the spectral width of the incident pulse. A noise  $i_n(t)$  proportional to the power of the LO and to the solar background irradiance is added.

$$i_n(t) \propto \sqrt{P_{cloud}^{sun} + P_{surf}^{sun} + P_{lo}}$$

The signal power is computed in each range gate  $\Delta R$  using the well known lidar equation (Eq 2, a and b). In these equations,  $P_0$  is the laser pulse power,  $S_{telesc}$  is the receiver surface,  $\eta_{opt}$  and  $\eta_{het}$  are the optics and heterodyne efficiency,  $O(R)$  is the laser-beam receiver-field-of-view overlap function,  $\beta(R, \lambda)$  is the backscatter coefficient,  $T(R)$  is the atmospheric transmission between the receiver and the range  $R$ ,  $A$  is the surface albedo ( $\pi \times$  reflectance). The power per time gate interval is computed by dividing each range

Figure 1: Example of down-looking observation geometry using two telescopes for measuring two orthogonal components of the horizontal winds in the same horizontal air slab.



gate into thin slices where the atmospheric properties are assumed constant. Equations 2 are applied to each slice, and the surface contribution is added to the slice that intercept the surface.

The background radiation due to solar irradiation is given by Eq. 2-c, where  $I_{sun}$  ( $Wm^{-2}\mu m^{-1}$ ) is the extraterrestrial irradiance spectral density,  $E$  is the solar zenith angle at the reflection point,  $\Delta\lambda$  is the receiver spectral bandwidth,  $\Omega = \pi \left(\frac{\theta}{2}\right)^2$  is the solid

$$\text{Eq. 2} \left\{ \begin{array}{ll} (a) & P_0 \frac{S_{telescope} O(r) \eta_{opt} \eta_{het} \beta(R, \lambda) T^2(R, \lambda) \Delta R}{R^2} \quad \text{for aerosol/cloud/molecular backscattering} \\ (b) & P_0 \frac{S_{telescope} O(R) \eta_{opt} \eta_{het} A T^2(R, \lambda)}{2\pi R^2} \quad \text{for surface reflection} \\ (c) & \frac{A I_{sun} \cos(E) S_{telescope} \Omega \Delta\lambda O(R) \eta_{opt} \eta_{het} T(R) T^{sun}(R)}{\pi} \quad \text{for surface/top-of-cloud solar reflection} \end{array} \right.$$

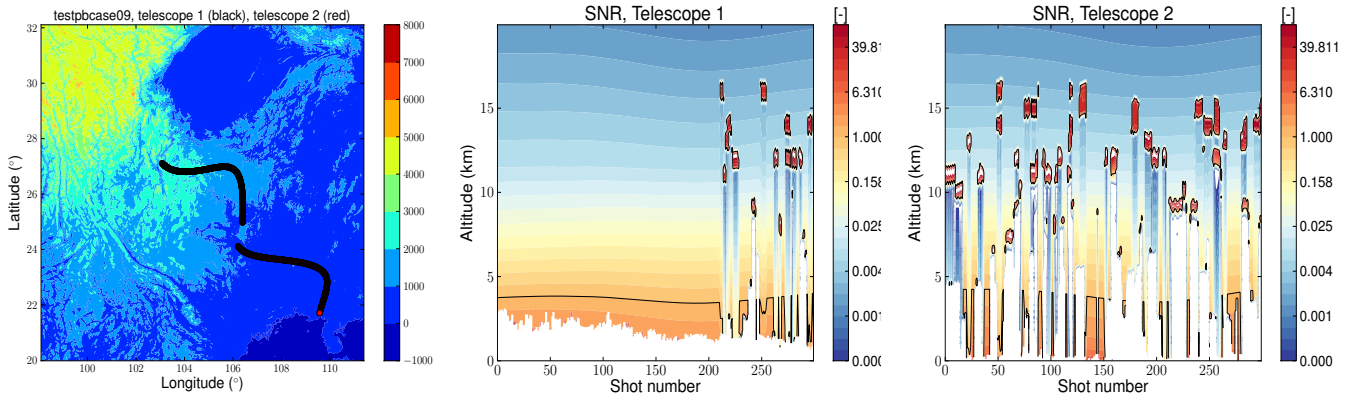
The atmospheric data are winds, temperature, pressure, humidity, aerosols and cloud distributions. They are taken from a three-dimensional global aerosol climate model [7]. The resolution is  $5.6^\circ \times 5.6^\circ$ . Aerosols are divided between 2 types of particles: type-1 (carbonate and sulfate) and type-2 (soil dust and seasalt). The model also provides liquid water content and coverage percentage for stratiform and cumiform cloud types.

The interactions between the laser pulses and the atmosphere are fully described by the backscatter coefficients and the transmission. The signal attenuation by air molecules includes absorption from the resonant spectral lines as well as an absorption con-

tinuum due to water-vapor and losses by Rayleigh scattering. The continuum and Rayleigh scattering parameters are taken from the model by Clough-Kneizys-Davies and the resonant line parameters are from the HITRAN catalog (1996). Scattering and absorption coefficients for aerosols particles and cloud droplets are derived from Mie scattering computation assuming homogeneously distributed spheres.

Figure 2 shows a simulation of 300 shots at  $2.06\mu m$  by two telescopes on a platform at an altitude of 500 km. The observed region is in the south-east of China. The pulse width is  $0.5\mu s$ , the pulse energy is 2 J and the frequency repetition of the pulses is 10 Hz. The track of the laser shots on the surface are shown

Figure 2: The left panel shows the footprint of the telescopes on the surface. The background color is the terrain elevation (m) [2]. The two other panels show the SNR for both telescopes, respectively. The black line indicates the level SNR=1. White regions correspond to SNR below  $10^{-4}$  or to altitudes below the Earth surface.



in the left panel. The separation of the two telescope footprints is about 500 km. A clear sky atmosphere is seen by the telescope 1 during the first 200 shots. The return signal is due to the presence of aerosols. A SNR of 1 for a single shot is obtained at the altitude of  $\sim 4$  km. The scenes seen by telescope 2 are more cloudy. The signal strongly increases within the cloud (SNR > 20) but decreases in the cloud shadow.

#### 4. Future improvements

Aerosols and clouds data will be updated using more recent model outputs (e.g., MASINGAR model from the Meteorological Res. Inst. in Tsukuba). Ice particles for high altitude cirrus clouds will be taken into account since they have a significant impact: ice particles scatter photons toward the receiver and, then increase the signal in the upper troposphere, but on the other hand, absorb the signal from lower altitudes. The computation of the extinction coefficient will include the case of non-spherical particles (e.g., T-matrix method). Currently, data for complex refractive indexes are only provided for the wavelength at  $2.06 \mu\text{m}$ , a database of the indexes in other spectral regions will be added. The possibility of computing the molecular absorption coefficient at any wavelength will be provided using a climatology of the atmospheric components (e.g.,  $\text{O}_3$ ,  $\text{CH}_4$ ). Parameters for line-by-line and continua models will be updated using the latest versions of the HITRAN spectroscopic database (2008) and the model by Mlawer-Tobin-Clough-Kneizys-Davies (MT-CKD,

2.5), respectively.

## References

- [1] Baker, W. E. et al.: Lidar-Measured Winds from Space: A Key Component for Weather and Climate Prediction, *Bull. Amer. Meteor. Soc.*, 76, 869–888, doi:10.1175/1520-0477(1995)076, 1995.
- [2] Becker, J. J. et al: Global Bathymetry and Elevation Data at 30 Arc Seconds Resolution: SRTM30 PLUS, *Marine Geodesy*, 32:4, 355–371, 2009.
- [3] Frehlich, R. G. et Yadlowsky, M. J.: Performance of mean-frequency estimators for Doppler radar/lidar, *J. Atmos. Ocean. Technol.*, 11, 1217–1230, 1994.
- [4] Ishii, S. et al: Coherent  $2 \mu\text{m}$  differential absorption and wind lidar with conductively cooled laser and two-axis scanning device, *Appl. Opt.*, 49, 1809–1817, 2010.
- [5] Kane, T. J. et al: Potential for coherent Doppler wind velocity lidars using neodymium lasers, *Appl. Opt.*, 23, 2477–2481, doi:10.1364/AO.23.002477, 1984.
- [6] Stoffelen, A. et al: The Atmospheric Dynamics Mission For Global Wind Field Measurement, *Bull. Amer. Meteor. Soc.*, 86, 73–87, 2005.
- [7] Takemura, T. et al: Global three-dimensional simulation of aerosol optical thickness distribution of various origins, *J. Geophys. Res.*, 105, 17853–17873, doi: 10.1029/2000JD900265, 2000.
- [8] Zagar, N. et al: Impact Assessment of Simulated Doppler Wind Lidars with a Multivariate Variational Assimilation in the Tropics, *Mon. Wea. Rev.*, 136, 2443–2460, doi: 10.1175/2007MWR2335.1, 2008.